Research Article | Vol. 10, No. 3 | 1 Mar 2019 | BIOMEDICAL OPTICS EXPRESS 1151
Biomedical Optics EXPRESS

Multimodal virtual histology of rabbit vocal folds by nonlinear microscopy and nano computed tomography

Alexei Kazarine,[1] Ksenia Kolosova,[2] Angelica A. Gopal,[1,3] Huijie Wang,[4,5] Rui Tahara,[6] Almoaidbellah Rammal,[7,8] Karen Kost,[7] Luc Mongeau,[4] Nicole Y. K. Li-Jessen[5,7,9] and Paul W. Wiseman[1,2,*]

[1]*Department of Chemistry, McGill University, 801 Sherbrooke St. West, Montreal, QC H3A 0B8, Canada*
[2]*Department of Physics, McGill University, 3600 University St., Montreal, QC, H3A 2T8, Canada*
[3]*Department of Physiology, McGill University, 3655 Promenade Sir William Osler, Montreal, H3G 1Y6, Canada*
[4]*Department of Mechanical Engineering, McGill University, 817 Sherbrooke St. West, Montreal, QC H3A 0C3, Canada*
[5]*School of Communication Sciences and Disorders, McGill University, 2001 McGill College Ave., Montreal, QC H3A 1G1, Canada*
[6]*Redpath Museum, McGill University, 859 Sherbrooke St. West, Montreal, QC H3A 0C4, Canada*
[7]*Department of Otolaryngology – Head and Neck Surgery, McGill University, 1001 Decarie Blvd., Montreal, QC, H4A 3J1, Canada*
[8]*Department of Otolaryngology – Head and Neck Surgery, King Abdul-Aziz University, Jeddah, Saudi Arabia*
[9]*Department of Biomedical Engineering, McGill University, 3775 University St., Montreal H3A 2B4, Canada*
**paul.wiseman@mcgill.ca*

Abstract: Human vocal folds (VFs) possess a unique anatomical structure and mechanical properties for human communication. However, VFs are prone to scarring as a consequence of overuse, injury, disease or surgery. Accumulation of scar tissue on VFs inhibits proper phonation and leads to partial or complete loss of voice, with significant consequences for the patient's quality of life. VF regeneration after scarring provides a significant challenge for tissue engineering therapies given the complexity of tissue microarchitecture. To establish an effective animal model for VF injury and scarring, new histological methods are required to visualize the wound repair process of the tissue in its three-dimensional native environment. In this work, we propose the use of a combination of nonlinear microscopy and nanotomography as contrast methods for virtual histology of rabbit VFs. We apply these methods to rabbit VF tissue to demonstrate their use as alternatives to conventional VF histology that may enable future clinical studies of this injury model.

1. Introduction

Human vocal folds have a distinctive tri-layered mucosal structure with rich extracellular matrix substances such as collagen, elastin and hyaluronan [1]. The delicate structure of the VFs makes them prone to scarring as a consequence of injury, disease or surgery [2]. The thicker scar tissue inhibits proper phonation and leads to voice disorders or even the loss of voice, which significantly hampers the patient's communicative ability and quality of life [3]. Surgical attempts to remove the scar often result in additional, iatrogenic scarring [4]. While studies have been conducted on potential therapies, effective treatment for the prevention or removal of VF scarring has not yet been achieved [5–8]. Proper understanding of the cellular mechanisms of the scarring process is required for the development of better treatment strategies [9].

#354722 https://doi.org/10.1364/BOE.10.001151
Journal © 2019 Received 13 Dec 2018; revised 29 Jan 2019; accepted 31 Jan 2019; published 11 Feb 2019

Biomedical Optics EXPRESS

Histology provides invaluable insight into both normal tissue physiology and disease pathology. The complex and heterogeneous structures of VF however present a unique challenge in histological analyses [10]. Histopathology remains largely unmodified since its introduction more than a century ago and continues to be based on the microscopic observation of micron-thin tissue slices stained with colored dyes. Hematoxylin and Eosin (H&E) staining, for example, has been employed since the 1800s [11]. Visualization of specific components of connective tissue can be performed using traditional immunoperoxidase or histochemical staining, such as reticulin (type III and IV collagen), Masson's trichrome (collagen and muscle), and the Verhoeff–van Gieson stain (elastic fibres and collagen) [12]. While conventional histology (Fig. 1(A)) provides important ultrastructural information at the micron level, the procedure is labor-intensive since it requires fine slicing of the tissue into thousands of individual slices, dyeing of the tissue, and manual microscopic observation of each slice to locate features of interest [13]. Since native tissues are organized in three-dimensional (3D) structures, a two-dimensional slice can only provide limited local information. To provide an improvement over conventional histology, new methodologies must be explored to enable high resolution three-dimensional visualization of tissue ultrastructure in a form of "virtual" histology. Among potential approaches, two imaging techniques, namely nano computed tomography (CT) and nonlinear microscopy (NM), show great promise towards addressing this challenge (Fig. 1B). While magnetic resonance imaging (MRI) has previously been used to study the scarring process of vocal fold mucosa in rats, the resolution provided by the technique is insufficient for ultrastructure visualization in three dimensions [14].

Nanotomography (also called Nano-CT) employs x-ray illumination to obtain cross sectional images of tissue as the sample is rotated on a moving stage [15]. Nano-CT's contrast is based on tissue density and sometimes enhanced with phosphotungstic acid staining when native tissue contrast is insufficient. Unlike traditional medical computed tomography or microtomography [16], nanotomography employs x-ray optics and small focal volumes to obtain isotropic submicron volume elements (voxels). Using this volumetric data, a virtual three-dimensional model of the sample can be reconstructed and "re-sliced" as desired for histological observation. Most recently, x-ray nanotomography has been used for 3D multiscale imaging of human vocal folds [17].

Nonlinear microscopy is a laser scanning imaging technique that exploits multiphoton absorption of infrared (IR) photons from ultrafast laser sources to enable deep tissue imaging [18]. This method offers a variety of label-free contrast mechanisms thanks to multiple simultaneous light-matter interactions that occur in the sample upon illumination with ultrashort laser pulses from IR lasers. Two photon autofluorescence (TPAF) imaging can reveal native intrinsic fluorophores in tissue such as elastin, NADH and hemoglobin amongst others [19]. Second harmonic generation (SHG) is a nonlinear scattering process in which two incident photons are combined into a single emitted photon having twice the incident laser light frequency [20]. This process can only occur in dense, non-centrosymmetric media and was initially discovered using inorganic crystalline materials. In biological tissue, SHG has been demonstrated to be significant in collagen and muscle and is now often used as the gold standard for collagen imaging [21]. We have previously utilized nonlinear microscopy to investigate tissue sections of human [22], rat [23], porcine [24,25], and rabbit vocal folds [26].

Traditional nonlinear microscopy enables imaging depths in biological tissues down to ~1 mm in the best case scenario, at which point it is significantly limited by scattering of the incident excitation beam [27]. To increase the imaging depth beyond a millimeter, new sample processing methods have been developed to significantly reduce tissue scattering [28]. These optical clearing techniques employ an immersion medium to reduce or eliminate refractive index differences between tissue components, rendering the tissue transparent. Refractive index matching is typically preceded by removal of lipids to reduce the refractive

Biomedical Optics EXPRESS

index of the tissue. Various optical clearing techniques have been developed, with key differences being the choice of delipidation method and refractive index matching solution [29]. Aqueous methods, such as CUBIC, are easy to implement and are compatible with a wide range of fluorescent dyes and proteins. Such methods are however limited to small samples, result in sample enlargement, and require significant preparation time [30]. To combat this, hydrogel embedding methods, such as CLARITY, have been developed that provide faster aqueous clearing of larger samples although at an increased cost [31]. Organic solvent-based methods such as uDISCO result in less expensive and faster tissue clearing [32]. However, the dehydration steps inherent in solvent based methods can often result in significant tissue shrinkage and loss of lipids. The choice of clearing method therefore directly depends on the desired application. For the purposes of virtual histology, uDISCO appears to be an optimal choice due to its low cost, high efficiency and good preservation of intrinsic fluorescent proteins. In combination with tissue clearing, nonlinear microscopy can provide mm^3 sized volumetric imaging with submicron lateral and micron-sized axial resolution, rendering it of great interest in virtual histology.

In this work, we present a new histological approach of combining nano-CT with nonlinear microscopy and uDISCO tissue clearing to obtain three-dimensional virtual models of the vocal folds. This virtual histology is important for determining normal vocal fold physiology prior to the establishment of a wound model for the study of vocal fold scarring and regeneration. In comparison with normal histology, our approach enables a three-dimensional view of the vocal fold ultrastructure, with easy determination of tissue features such as the cartilage, lamina propria layers, muscles and blood capillaries that are important structures to visualize for wound healing studies. The volume renders can easily be separated into cross sectional planes that are familiar to anatomic pathologists, enabling detailed observation of regions of interest.

This study represents the first instance of whole rabbit vocal fold histological imaging, enabled by optical clearing, nonlinear microscopy, and nano-CT. This new, integrated histological approach could bring significant insights in the three-dimensional anatomical organization and physiology of normal and diseased vocal fold tissues, which has traditionally only been examined in two dimensions through irreversible mechanical sectioning of tissue slices.

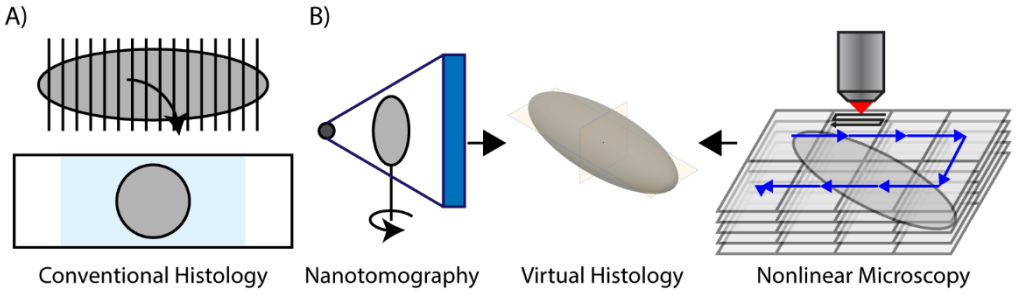

Fig. 1. Schematic comparison of the concepts of conventional histology (A) with virtual histology by nanotomography and nonlinear microscopy (B).

2. Materials and methods

2.1 Animal study

Ethics approval was obtained from the McGill University Animal Care Committee (Protocol number DOW FACCs 2014-7556). All animal handling and experimental procedures were carried out in accordance with the National Institutes of Health (NIH) guidelines for care and use of laboratory animals. A rabbit model was selected as it is a well-documented model commonly used to study vocal fold injuries [33]. Rabbits possess larger vocal folds than

Biomedical Optics EXPRESS

smaller laboratory animals such as rats [34], enabling easier and more reliable vocal fold surgery. For the purposes of this study, one New Zealand white rabbit received a surgical injury on the left vocal fold while the right was kept intact as a control.

The animal was sacrificed 42 days after surgical intervention and its larynx was excised for ex-vivo high resolution nano-CT and nonlinear microscopy imaging. For coarse, full size CT imaging, one intact rabbit larynx was excised from a rabbit carcass obtained from a commercial source.

2.2 Tissue clearing

For nonlinear microscopy, the vocal cords were dissected from the rabbit larynx sample to reduce tissue thickness to 2 mm to match the microscope objective working distance. Optical clearing was conducted using the established uDISCO clearing protocol [32]. Laboratory reagents were obtained from Millipore Sigma (ON, Canada) unless otherwise indicated. Briefly, the sample was first dehydrated through sequential passages in 30%, 50%, 70%, 80%, 90%, 96% v/v tert-butanol solutions in distilled water before incubation in a refractive index matching solution consisting of a mixture of benzyl alcohol (BA), benzyl benzoate (BB) and diphenyl ether (DPE) in a 2:1:4 (BA-BB-DPE) v/v solution. Concurrently, α-tocopherol was added at a final concentration of 0.4% v/v as an oxygen scavenger. Each clearing step was maintained for one day at room temperature. Figure 2(A) shows the rabbit vocal folds after dissection while Fig. 2(B) shows the same sample after optical clearing.

Custom imaging chambers were designed and fabricated to allow a complete encapsulation of the sample immersed in the refractive index matching solution while avoiding physical contact with the microscope objective during nonlinear imaging. The chambers consist of polydimethylsiloxane (PDMS) spacers cast from a machined aluminum mold that were attached to microscope slides during the casting process, resulting in a permanent bond. Once the sample is introduced to the chamber, enough refractive index matching solution is added to slightly overfill the chamber and a no. 1.5 coverslip was then used to close the chamber and ensure a seal by surface tension. The isolated sample could then be safely manipulated and imaged by nonlinear microscopy. A render of the sample encapsulated in a chamber is shown in Fig. 2©.

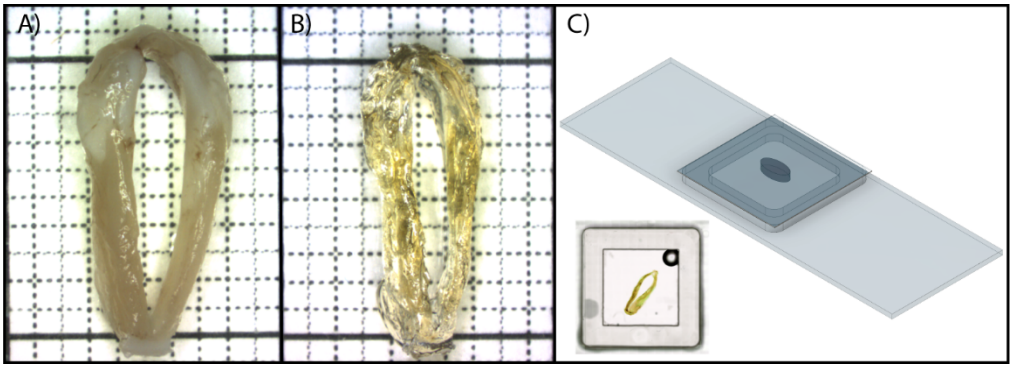

Fig. 2. Optical clearing of rabbit vocal folds. (A) Uncleared vocal fold tissue after dissection, (B) the same tissue after clearing with the uDISCO protocol, (C) render of imaging chamber used for nonlinear microscopy of the cleared tissue, inset showing brightfield microscopy image of the sample and chamber. Dotted lines in (A) and (B) are spaced 1mm apart.

2.3 Nanotomography

For coarse nanotomography, a full rabbit larynx was dissected, dehydrated with passages to 70% ethanol and stained with an alcoholic solution of phosphotungstic acid (PTA) to enhance soft tissue contrast [35]. For high resolution nanotomography, the same rabbit larynx sample

Biomedical Optics EXPRESS

that was previously optically cleared and imaged by nonlinear microscopy was immersed in ethanol passages to 70% ethanol before PTA staining.

Nanotomography was conducted using a Zeiss Xradia Versa 520 x-ray microscope (Carl Zeiss Canada Ltd., ON, Canada). For full laryngeal imaging, an optical magnification of 0.4x was used to achieve an isotropic voxel size of 12 µm. For high resolution imaging of the rabbit vocal fold, a 4x optical magnification was employed for a final voxel size of 0.8 µm. Virtual models of the nanotomography image stacks were created and analyzed using Dragonfly (Object Research Systems, QC, Canada). This software enabled easy determination of cross sectional planes by directly selecting corresponding x/y/z axes after volume rendering.

2.4 Nonlinear microscopy

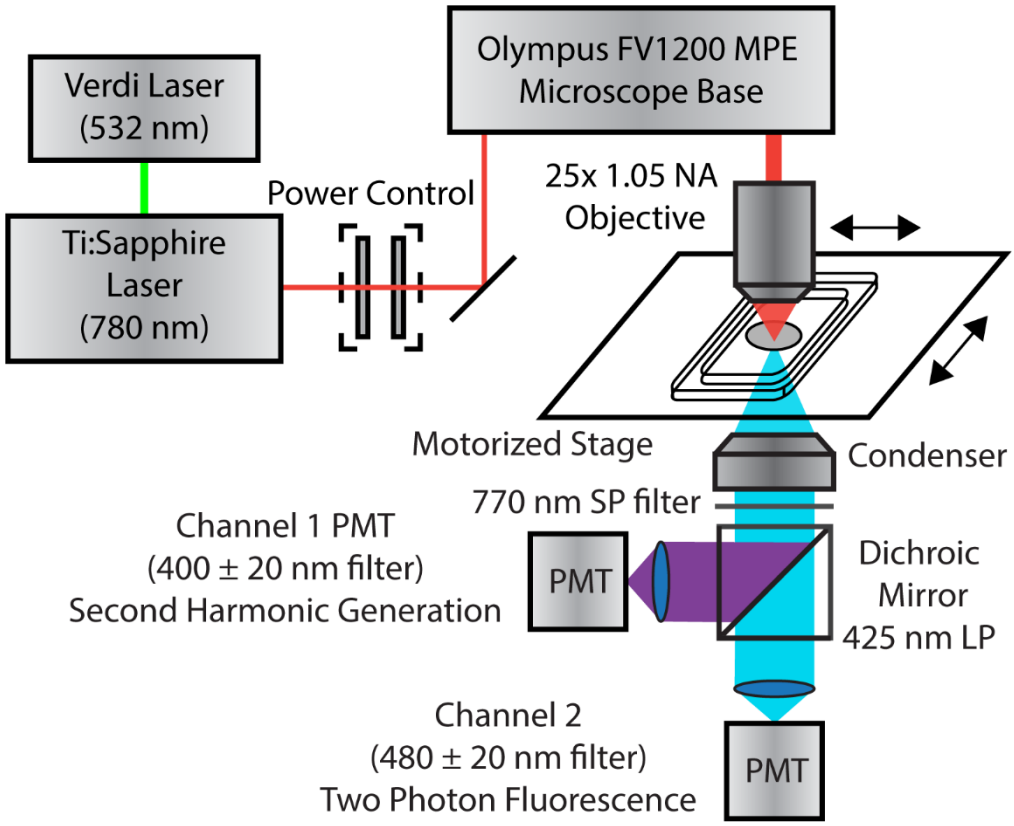

Fig. 3. A schematic diagram of the nonlinear microscopy imaging system. The Verdi (532 nm) laser pumps the Ti:Sapphire laser (780 nm) that is directed into the microscope base with computer control over the power. A 25X 1.05NA water immersion objective is used to focus the excitation light onto the sample. Forward detection was achieved using a condenser lens, where the emission was separated into two channels: the second harmonic generation channel (Channel 1) and the two-photon fluorescence channel (Channel 2) and subsequently detected by photomultipliers (PMTs).

Nonlinear microscopy was performed using a customized multiphoton microscope (Fig. 3) based on a FV1200 MPE microscope base (Olympus Canada Inc, ON, Canada). Excitation with 780 nm laser light was achieved by a Ti:Sapphire laser (Mira 900F, Coherent, CA) pumped by a 532 nm laser (Verdi V18, Coherent, CA). The excitation laser provided 200 fs pulses at a 76 MHz repetition rate. Laser power was measured, and computer controlled immediately prior to entry to the microscope by a custom built variable attenuator consisting of a rhomb retarder (FR600HM, Thorlabs, NJ) mounted on a motorized rotational stage

Biomedical Optics EXPRESS

(PRM1Z8, Thorlabs, NJ, USA) and a linear Glan-Laser polarizer (GL10, Thorlabs, NJ). Imaging was conducted using a 25x 1.05 NA water immersion objective (XLPL25XWMP(F), Olympus Canada Inc, ON, Canada) with a working distance of 2 mm. Emission light was collected with a dry top lens condenser, split by a long pass (LP) dichroic mirror (T425lpxr, Chroma Technology, VT) and directed into two detection photomultipliers (PMTs) for simultaneous detection of second harmonic generation (380-420 nm filter, ET400/40x, Chroma Technology, VT) and two-photon fluorescence (460-500 nm filter, BA 460-500, Olympus Canada Inc, ON, Canada). A 770 nm IR blocking short pass (SP) filter (FF01-770/SP32, Semrock, NY) was placed immediately below the condenser to prevent the excitation light from reaching the detectors. The sample was mounted on a motorized stage to conduct three-dimensional mosaic imaging. Adjacent image fields were stitched using Fluoview (Olympus Canada Inc, ON, Canada) to obtain 3D image stacks, that were rendered as virtual models in Imaris (Bitplane Inc., South Windsor, CT) and Dragonfly (Object Research Systems, QC, Canada).

3. Results and discussion

Virtual histology combines the principles of optical sectioning and three-dimensional volume rendering to obtain high resolution histological information from intact tissue. Instead of physical slicing, virtual slicing through the rendering software allows easy manipulation for rapid interpretation of histological data. With recent advances in both central and graphical processing unit technology, computing power has become inexpensive enough for such rendering to be done on standard desktop workstations. To compete with conventional histology of vocal folds, virtual histology methods must present similar resolution and contrast along with deep tissue penetration to enable efficient 3D data collection.

Three-dimensional histology of animal vocal folds is critical in establishing their use as a wound healing model for vocal fold injury and repair. While the rabbit model has been used to evaluate different potential vocal fold regeneration therapies [36], the data obtained in these studies was limited to traditional histology such as H&E, which cannot provide the entire three-dimensional tissue landscape when it comes to a spatial understanding of wound healing. By using virtual histology, the entire wound area could be observed and compared across animals over time. Such capability is important to standardize the location and size of the injury and to evaluate the wound healing outcome in a more consistent manner. Before such studies can be conducted, it is important to determine the ultrastructure of normal rabbit vocal folds and verify that the proposed virtual histology methods provide adequate resolution and contrast. To achieve this, we have evaluated two potential avenues for conducting virtual histology of rabbit vocal fold tissue: nanotomography and nonlinear microscopy, each of which presents its own advantages and limitations.

3.1 Virtual histology of an entire rabbit larynx via nanotomography

Nanotomography employs a combination of a rotating stage with x-ray imaging and computer processing to obtain a three-dimensional image stack with a final submicron voxel size and contrast based on tissue density. The flexibility of this system lies in its ability to image large samples at varying resolution, allowing us to capture both lower resolution coarse renders of entire organs followed by detailed submicron resolution imaging of volumes of interest.

We first imaged an entire rabbit larynx using a coarser magnification (12 μm^3 voxels) to obtain a render of the entire vocal folds and their surrounding tissues (Fig. 4A). In the transverse plane (Fig. 4B), the vocal folds and surrounding cartilage are immediately visible, with easy software-controlled sectioning enabling discrete observation of the tissue types.

Biomedical Optics EXPRESS

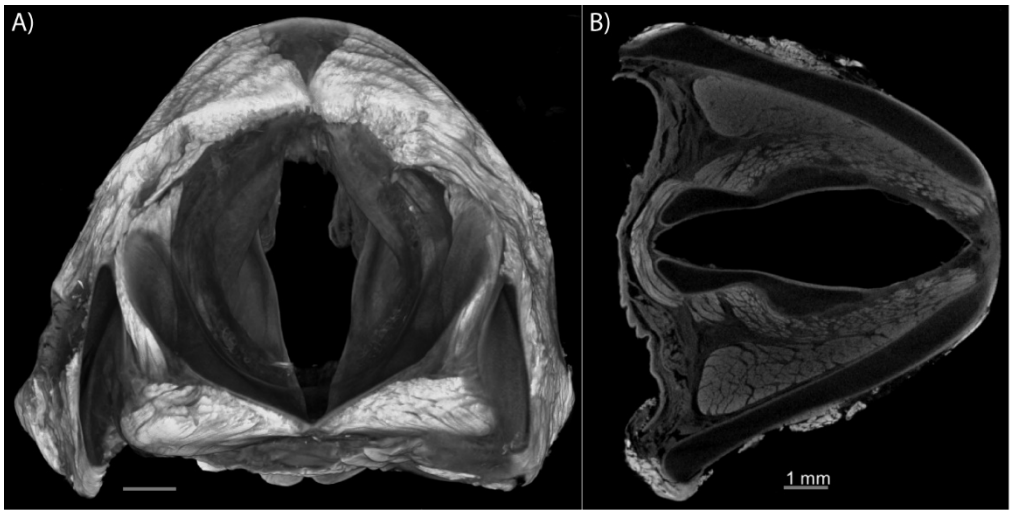

Fig. 4. Coarse tomography of a rabbit larynx. (A) 3D volume render of the entire rabbit larynx. (B) Cross sectional plane across the rabbit larynx. Scale bars are 1 mm.

Fig. 5. Comparison of histology methods applied to rabbit vocal folds. (A) Virtual histology by Nano-CT. (B) Classical histology example by hematoxylin and eosin staining of a thin tissue slice of rabbit larynx. White arrow indicates the vocal fold lamina propria, yellow arrow points to muscle while the magenta arrow denotes an area of cartilage. Scale bars are 1 mm.

Figure 5 demonstrates a comparison between virtual histology with coarse nanotomography (Fig. 5(A)) and classical histology with H&E staining (Fig. 5(B)) for coronal sections of vocal fold tissue. In H&E sections, the contrast is provided by tissue components that are either basophilic or acidophilic, resulting in color differences between dark purple (cell nuclei) and pink (cytoplasm and extracellular matrix components). Using tomography, the tissue components are contrast distinguished by their density, with adequate separation in signal levels between cartilage, muscle and the soft tissue of the vocal fold lamina propria (basement membrane) that can be easily distinguished (Fig. 5(A)).

3.2 Virtual histology of a dissected rabbit larynx via nonlinear microscopy and nanotomography

Nonlinear microscopy is a deep tissue optical imaging technique commonly used for the observation of thick specimens. By using femtosecond pulsed near-infrared excitation lasers,

Biomedical Optics EXPRESS

nonlinear microscopy allows for inherent optical sectioning and an imaging depth of nearly 1 mm before loss of signal due to scattering and attenuation.

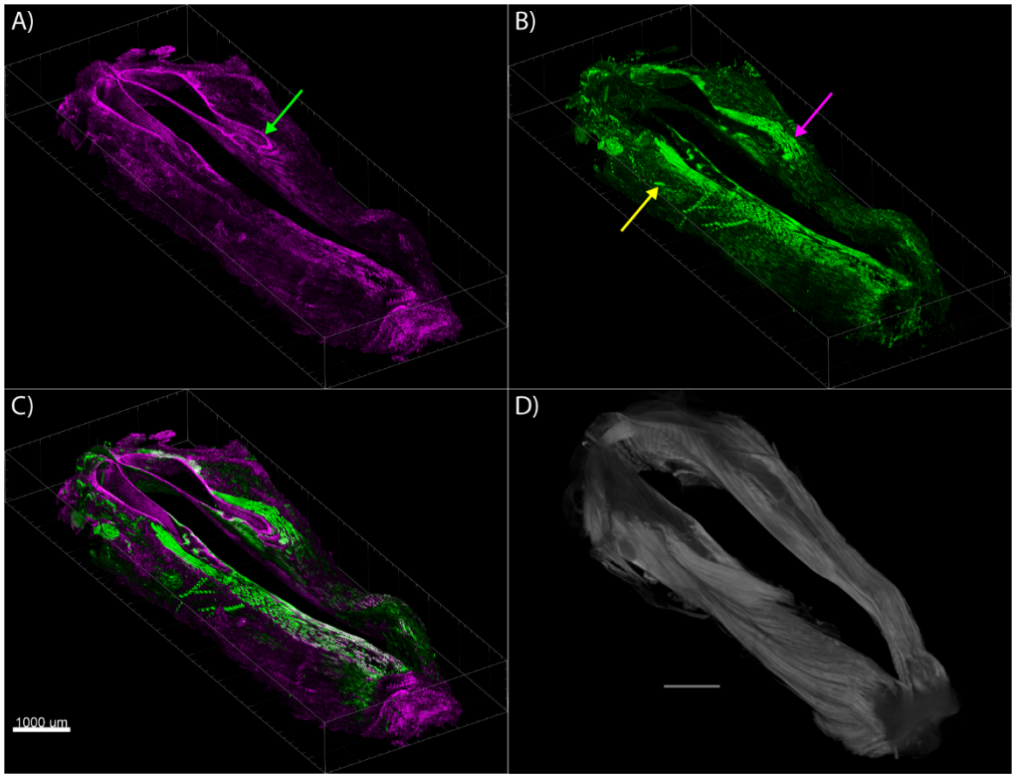

Fig. 6. 3D volume render of dissected rabbit vocal folds imaged by nonlinear microscopy and nanotomography (coarse). (A) Channel 1: Second Harmonic Generation highlighting collagen type I & III fibers. Green arrow highlights structural laryngeal cartilage. (B) Channel 2: Two Photon Autofluorescence showing primarily muscle cell NADH (magenta arrow) and blood vessel (yellow arrow). (C) Composite of (A) and (B). (D) Coarse nanotomography of the same dissected rabbit larynx performed after nonlinear microscopy. (A-C) are at the same scale. Scale bars are 1 mm.

This imaging depth can be significantly extended using optical clearing techniques, which render the tissue transparent and greatly reduce scattering and excitation power loss. If adequate tissue clearing is performed, the imaging depth is then only limited by the working distance of the microscope objective. In our study, we used the uDISCO clearing protocol to obtain rapid optical clearing of rabbit vocal fold tissue in less than a week. Due to the 2 mm working distance of our objective lens, the rabbit larynx sample was first dissected to fit this size before imaging via nonlinear microscopy.

To compare nonlinear microscopy to nanotomography on the same sample, we first performed nonlinear imaging on an unlabeled rabbit larynx sample using SHG and TPAF imaging, two contrast mechanisms that exploit inherent tissue properties. SHG allows the visualization of collagen type I & III fibers [37] in vocal folds, while TPAF centered around emission wavelength of 480 nm highlights elastic fibers and NADH in muscle cells [18]. After nonlinear imaging, we passaged the sample into ethanol to prepare it for nanotomography.

Full size volume renders of the vocal folds and surrounding tissue imaged by nonlinear microscopy and coarse nanotomography can be found in Fig. 6. Nonlinear imaging was performed at x-y pixel sizes of 0.5 µm with 50 µm steps between z slices, while the coarse nanotomography utilized a voxel size of 12 µm. The contrast difference between nonlinear

Biomedical Optics EXPRESS

microscopy (Fig. 6(A)-(C)) and nanotomography (Fig. 6(D)) is directly visible even at the coarse resolution utilized in nanotomography. The SHG volume (Fig. 6(A)) highlights the collagen structure of the laryngeal cartilage and within the VF lamina propria. The TPAF render (Fig. 6(B)) primarily shows muscle fibers via autofluorescence of NADH along with evidence of blood vessels via red blood cell and elastic lining autofluorescence.

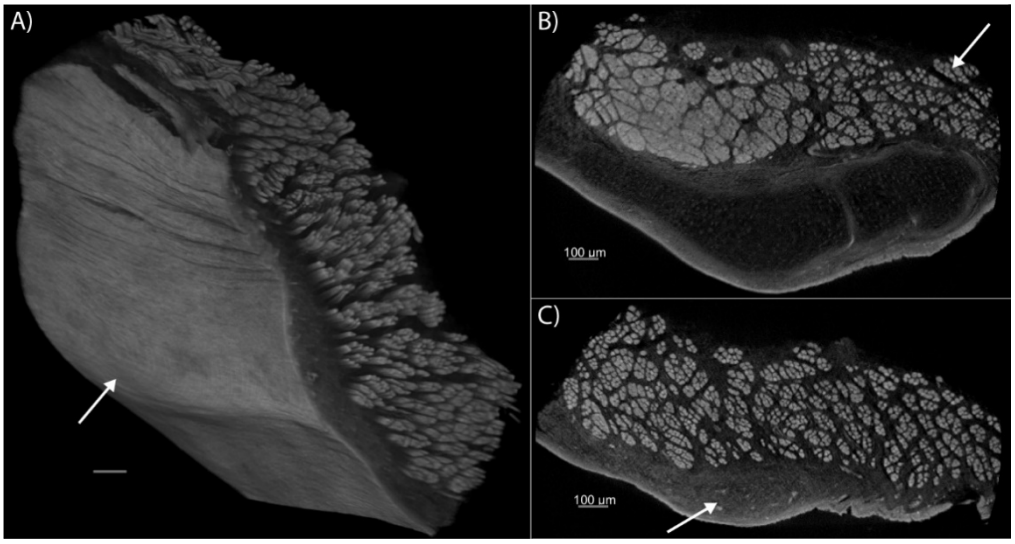

Fig. 7. High resolution nanotomography of rabbit vocal fold tissue and the surrounding area. (A) 3D volume render of the epithelium (highlighted by white arrow), vocal fold lamina propria, and surrounding muscle. (B) Cross section of cartilage and muscle (highlighted by white arrow) in the surrounding tissue of the vocal fold. (C) Vocal fold lamina propria (white arrow) cross section. Scale bars are 100 µm.

3.3 Tissue ultrastructure revealed by high resolution nanotomography

Nanotomography of the dissected rabbit vocal folds (see Fig. 6(D)) was first performed at a coarse resolution with a voxel size of 12 µm to facilitate fast visualization of the vocal fold and surrounding tissues for a broad overview of the sample. Using this overview, the vocal fold volumes were identified and re-imaged at high resolution (0.8 µm voxel size) to push the resolution limits of nanotomography (Fig. 7(A)). When virtually cross-sectioned, the resulting volume allows easy observation of both cartilage (Fig. 7(B)) and vocal fold histology (Fig. 7(C)), including epithelium, lamina propria and muscle fibers. This demonstrates the powerful capabilities of nanotomography to visualize tissue ultrastructure directly at a three-dimensional level without destruction of the delicate VF tissue from its native state.

The main limitation of nano-CT lies in its contrast mechanism, which is based on tissue density. Staining can enhance the contrast at the soft tissue level and enable differentiation between major tissue types, similarly to the contrast obtained using H&E staining. However, without immunolabeling, neither of these techniques can provide the specificity to highlight single protein targets.

3.4 Cellular details revealed by high resolution nonlinear microscopy

We also conducted high resolution nonlinear imaging of the rabbit vocal fold tissue with z-spacing of 1 µm (Fig. 8). In the full render (Fig. 8(A)), the ultrastructure of the rabbit vocal fold is directly visible, as the two contrast mechanisms highlight different layers of the tissue, including the epithelium, lamina propria (basement membrane), collagen fibers and muscle tissue.

Biomedical Optics EXPRESS

In the high-resolution images obtained, several tissue features are directly revealed at the cellular level. In the 480 nm detection channel, TPAF demonstrates the presence of red blood cells in a blood vessel and NADH from cells in muscle tissue (Fig. 8(B)) along with chondrocytes and elastic fibers in the vocal fold cartilage (Fig. 8(C)). In the 400 nm detection channel, SHG from collagen fibers and the muscle tissue itself can be seen (Fig. 8(D)) along with collagen fibers and three photon fluorescence from elastic fibers visible in the cartilage. The elastic tissue shows direct correspondence between the two channels, allowing it to be distinguished from collagen fibers, which are only visible in the 400 nm channel.

The visualization of collagen fibers by SHG is dependent on the orientation of the fibers in relation to the polarization of the excitation beam. Consequently, by tightly controlling the linear polarization of the beam, the collagen structure could be further analyzed to reveal fiber orientation and aggregation [38]. This feature is beneficial for developing quantitative measures or biomarkers to characterize and monitor the health state of the tissue, such as scarring index.

Our utilization of solvent based optical clearing shrank the tissue in addition to optically clearing the tissue for deep imaging, resulting in decreased structural resolution. An approach to counteract this effect could be the use of expansion microscopy [39]. This technique utilizes polymers to expand tissues for improved visualization of smaller structures that are hidden by the diffraction limit. The implementation of expansion microscopy on entire vocal folds would however be limited by the working distance of the objective, as expanding the tissue will enlarge the sample beyond the range we could safely mount and image with our current microscope.

Other techniques that can be used to improve the optical resolution of imaging include the use of Bessel beams in two photon microscopy to improve lateral resolution at the expense of axial resolution [40]. To improve the resolution of 3D imaging, a light sheet approach can be utilized using Bessel-beam illumination, in both one [41] and two [42] photon regimes, which can also be combined with localization algorithms for super-resolution measurements [43].

While the rabbit used for the high-resolution CT and NM imaging received a surgical injury on the left vocal fold, we were unable to find any histological differences between the two vocal folds in either nano-CT, nonlinear microscopy images or traditional H&E examination. As such, the CT and NM images presented in this paper were from the uninjured right vocal fold. It is highly likely that the wounded VF had completely healed within the 42 days following the surgery without any significant tissue remodeling, which has been previously reported after 14 days post injury [44]. In this demonstration study, we have focused on exploring the normal rabbit vocal fold physiology in its native 3D form for the first time.

Future studies will be focused on quantitatively evaluating different injury models at earlier time points. We anticipate our novel approach to be of significant value in establishing vocal fold injury models as it would considerably aid in the localization of the wound site given its 3D capability. Previous studies have focused on 2D localization of vocal fold injuries with traditional histology that does not provide a complete picture of the 3D wound site and tissue remodeling. The application presented in this study uses commercially available technology in combination with inexpensive optical clearing, making it easily accessible to the medical research community.

Biomedical Optics EXPRESS

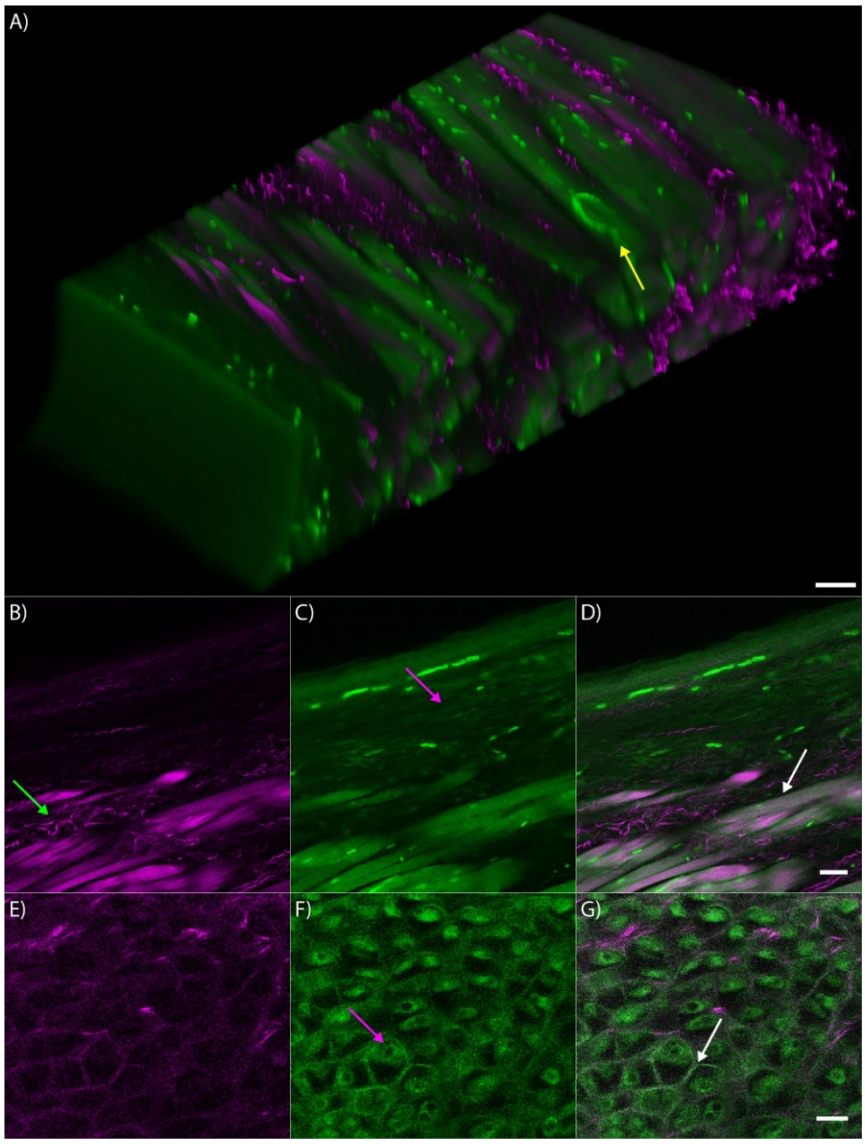

Fig. 8. High resolution nonlinear microscopy of optically cleared rabbit vocal fold and surrounding tissue. (A) 3D Volume render combining SHG (magenta) and TPAF (green), yellow arrow highlights the presence of red blood cells via autofluorescence from hemoglobin. (B-D) Imaged area including structural collagen (green arrow in SHG channel B), vocal fold lamina propria (magenta arrow in TPAF channel C), and surrounding muscle fibers (white arrow in composite D). (E-G) Imaged area showing surrounding cartilage, where E is the SHG channel, F is the TPAF channel highlighting chondrocytes (magenta arrow), and composite G shows presence of elastic fibers (white arrow). Scale bars are 25 µm.

In a comparison of both approaches as contrast methods for virtual histology of rabbit vocal folds, we were able to demonstrate that these techniques can be used in parallel to provide a complete picture of vocal fold histology. Nanotomography offers a convenient way of providing a coarse overview that can then be re-imaged at submicron resolution to obtain finer details of the relevant tissue ultrastructure. However, the density-based contrast mechanism in PTA labelled samples is an important limitation for the analysis of soft tissue as there is reduced contrast between cells in the vocal fold lamina propria and extracellular matrix components such as collagen and elastin. Nonlinear microscopy of cleared tissue can

Biomedical Optics EXPRESS

fill in these knowledge gaps as we were able to directly visualize collagen and elastin and resolve single cells at optical resolution in the same sample. While nonlinear microscopy shows a wealth of detailed histological information, it presents limitations due to the optical point spread function of the laser scanning microscope, which is diffraction limited to around 1 μm axially in size in this study. This limits the resolution in XZ and YZ cross-sectional planes in rendering. However, this limitation could be addressed by the implementation of nonlinear tomography [45] which rotates the sample as it is imaged to exploit the increased lateral resolution in XY for an isometric pixel reconstruction. Despite this limitation, label free nonlinear microscopy allows virtual histological evaluation of tissue features that directly rival those offered by conventional histology. In addition, the uDISCO technique is directly compatible with fluorescent antibody labelling along with the use of fluorescent proteins from transgenic animals, allowing for highly specific labelling of proteins of interest in a three-dimensional environment.

4. Conclusion

In this work, we presented a new approach to rabbit vocal fold virtual histology using a complementary combination of nanotomography and nonlinear microscopy. Using these two techniques, detailed 3D volume renders of rabbit vocal folds were constructed for the first time, which highlighted relevant tissue features for the study of vocal fold regeneration. The ultrastructural information obtained was comparable to traditional histology for the study of connective tissue but does not require tissue sectioning. Using this novel combination of methods, a rabbit vocal fold wound model could then be studied in its native 3D state, and quantitative evaluation of experimental wound repair treatments could be conducted.

Funding

National Sciences and Engineering Research Council of Canada (NSERC) (RGPIN-2017-05005, RGPIN-2018-03843); Canada Research Chair (Tier 2 – Canadian Institutes of Health Research); Canada Foundation for Innovation (229251, 33122); National Institutes of Health (NIH) (NIH DC 005788-15)

Acknowledgments

We thank David L. Kolin (M.D., Ph.D.) for his helpful comments and suggestions on this manuscript. We acknowledge the Integrative Quantitative Biology Initiative (IQBI) of McGill University for access to the Zeiss Xradia Versa 520. 3D rendering via Imaris for this work was performed in the McGill University Life Sciences Complex Advanced Biomaging Facility (ABIF).

Disclosures

The authors declare that there are no conflicts of interest related to this article.

References

1. M. Hirano, “Morphological Structure of the Vocal Cord as a Vibrator and its Variations,” Folia Phoniatr. (Basel) **26**(2), 89–94 (1974).
2. M. S. Benninger, D. Alessi, S. Archer, R. Bastian, C. Ford, J. Koufman, R. T. Sataloff, J. R. Spiegel, and P. Woo, “Vocal fold scarring: current concepts and management,” Otolaryngol. Head Neck Surg. **115**(5), 474–482 (1996).
3. S. Krischke, S. Weigelt, U. Hoppe, V. Köllner, M. Klotz, U. Eysholdt, and F. Rosanowski, “Quality of life in dysphonic patients,” J. Voice **19**(1), 132–137 (2005).
4. G. Friedrich, F. G. Dikkers, C. Arens, M. Remacle, M. Hess, A. Giovanni, S. Duflo, A. Hantzakos, V. Bachy, and M. Gugatschka; European Laryngological Society. Phonosurgery Committee, “Vocal fold scars: current concepts and future directions. Consensus report of the Phonosurgery Committee of the European Laryngological Society,” Eur. Arch. Otorhinolaryngol. **270**(9), 2491–2507 (2013).
5. A. Mattei, J. Magalon, B. Bertrand, C. Philandrianos, J. Veran, and A. Giovanni, “Cell therapy and vocal fold scarring,” Eur. Ann. Otorhinolaryngol. Head Neck Dis. **134**(5), 339–345 (2017).

Biomedical Optics EXPRESS

6. S. Hirano, "Current treatment of vocal fold scarring," Curr. Opin. Otolaryngol. Head Neck Surg. **13**(3), 143–147 (2005).
7. J. K. Hansen and S. L. Thibeault, "Current understanding and review of the literature: vocal fold scarring," J. Voice **20**(1), 110–120 (2006).
8. W. Chen, P. Woo, and T. Murry, "Vocal Fold Vibration Following Surgical Intervention in Three Vocal Pathologies: A Preliminary Study," J. Voice **31**(5), 610–614 (2017).
9. L. E. Tracy, R. A. Minasian, and E. J. Caterson, "Extracellular Matrix and Dermal Fibroblast Function in the Healing Wound," Adv. Wound Care (New Rochelle) **5**(3), 119–136 (2016).
10. B. Rousseau, S. Hirano, R. W. Chan, N. V. Welham, S. L. Thibeault, C. N. Ford, and D. M. Bless, "Characterization of chronic vocal fold scarring in a rabbit model," J. Voice **18**(1), 116–124 (2004).
11. M. Titford, "The long history of hematoxylin," Biotech. Histochem. **80**(2), 73–78 (2005).
12. S. C. Lester, *Manual of Surgical Pathology E-Book* (Elsevier Health Sciences, 2010).
13. K. S. Suvarna, C. Layton, and J. D. Bancroft, *Bancroft's Theory and Practice of Histological Techniques E-Book* (Elsevier Health Sciences, 2018).
14. A. O. Kishimoto, Y. Kishimoto, D. L. Young, J. Zhang, I. J. Rowland, and N. V. Welham, "High- and ultrahigh-field magnetic resonance imaging of naïve, injured and scarred vocal fold mucosae in rats," Dis. Model. Mech. **9**(11), 1397–1403 (2016).
15. P. J. Withers, "X-ray nanotomography," Mater. Today **10**(12), 26–34 (2007).
16. M. Senter-Zapata, K. Patel, P. A. Bautista, M. Griffin, J. Michaelson, and Y. Yagi, "The role of micro-CT in 3D histology imaging," Pathobiology **83**(2-3), 140–147 (2016).
17. L. Bailly, T. Cochereau, L. Orgéas, N. Henrich Bernardoni, S. Rolland du Roscoat, A. McLeer-Florin, Y. Robert, X. Laval, T. Laurencin, P. Chaffanjon, B. Fayard, and E. Boller, "3D multiscale imaging of human vocal folds using synchrotron X-ray microtomography in phase retrieval mode," Sci. Rep. **8**(1), 14003 (2018).
18. W. R. Zipfel, R. M. Williams, R. Christie, A. Y. Nikitin, B. T. Hyman, and W. W. Webb, "Live tissue intrinsic emission microscopy using multiphoton-excited native fluorescence and second harmonic generation," Proc. Natl. Acad. Sci. U.S.A. **100**(12), 7075–7080 (2003).
19. W. R. Zipfel, R. M. Williams, R. Christie, A. Y. Nikitin, B. T. Hyman, and W. W. Webb, "Live tissue intrinsic emission microscopy using multiphoton-excited native fluorescence and second harmonic generation," Proc. Natl. Acad. Sci. U.S.A. **100**(12), 7075–7080 (2003).
20. P. J. Campagnola and L. M. Loew, "Second-harmonic imaging microscopy for visualizing biomolecular arrays in cells, tissues and organisms," Nat. Biotechnol. **21**(11), 1356–1360 (2003).
21. P. J. Campagnola and X. Chen, "SHG Microscopy and Its Comparison with THG, CARS, and Multiphoton Excited Fluorescence Imaging," in *Second Harmonic Generation Imaging* (CRC Press, 2016), pp. 100–119.
22. A. K. Miri, U. Tripathy, L. Mongeau, and P. W. Wiseman, "Nonlinear laser scanning microscopy of human vocal folds," Laryngoscope **122**(2), 356–363 (2012).
23. H. K. Heris, A. K. Miri, N. R. Ghattamaneni, N. Y. Li, S. L. Thibeault, P. W. Wiseman, and L. Mongeau, "Microstructural and mechanical characterization of scarred vocal folds," J. Biomech. **48**(4), 708–711 (2015).
24. A. K. Miri, H. K. Heris, U. Tripathy, P. W. Wiseman, and L. Mongeau, "Microstructural characterization of vocal folds toward a strain-energy model of collagen remodeling," Acta Biomater. **9**(8), 7957–7967 (2013).
25. H. K. Heris, A. K. Miri, U. Tripathy, F. Barthelat, and L. Mongeau, "Indentation of poroviscoelastic vocal fold tissue using an atomic force microscope," J. Mech. Behav. Biomed. Mater. **28**, 383–392 (2013).
26. A. Kazarine, S. Bouhabel, A. H. Douillette, K. Kost, N. Y. K. Li-Jessen, L. Mongeau, and P. W. Wiseman, "Multimodal imaging of vocal fold scarring in a rabbit model by multiphoton microscopy," in *SPIE BiOS*, (SPIE, 2017), 9.
27. P. Theer and W. Denk, "On the fundamental imaging-depth limit in two-photon microscopy," J. Opt. Soc. Am. A **23**(12), 3139–3149 (2006).
28. P. Ariel, "A beginner's guide to tissue clearing," Int. J. Biochem. Cell Biol. **84**, 35–39 (2017).
29. D. S. Richardson and J. W. Lichtman, "Clarifying Tissue Clearing," Cell **162**(2), 246–257 (2015).
30. K. Tainaka, S. I. Kubota, T. Q. Suyama, E. A. Susaki, D. Perrin, M. Ukai-Tadenuma, H. Ukai, and H. R. Ueda, "Whole-body imaging with single-cell resolution by tissue decolorization," Cell **159**(4), 911–924 (2014).
31. R. Tomer, L. Ye, B. Hsueh, and K. Deisseroth, "Advanced CLARITY for rapid and high-resolution imaging of intact tissues," Nat. Protoc. **9**(7), 1682–1697 (2014).
32. C. Pan, R. Cai, F. P. Quacquarelli, A. Ghasemigharagoz, A. Lourbopoulos, P. Matryba, N. Plesnila, M. Dichgans, F. Hellal, and A. Ertürk, "Shrinkage-mediated imaging of entire organs and organisms using uDISCO," Nat. Methods **13**(10), 859–867 (2016).
33. A. M. Campagnolo, D. H. Tsuji, L. U. Sennes, R. Imamura, and P. H. Saldiva, "Histologic study of acute vocal fold wound healing after corticosteroid injection in a rabbit model," Ann. Otol. Rhinol. Laryngol. **119**(2), 133–139 (2010).
34. J. M. Coppoolse, T. G. Van Kooten, H. K. Heris, L. Mongeau, N. Y. Li, S. L. Thibeault, J. Pitaro, O. Akinpelu, and S. J. Daniel, "An in vivo study of composite microgels based on hyaluronic acid and gelatin for the reconstruction of surgically injured rat vocal folds," J. Speech Lang. Hear. Res. **57**(2), S658–S673 (2014).
35. B. D. Metscher, "MicroCT for developmental biology: a versatile tool for high-contrast 3D imaging at histological resolutions," Dev. Dyn. **238**(3), 632–640 (2009).

Biomedical Optics EXPRESS

36. M. J. Ban, J. H. Park, J. W. Kim, K. N. Park, J. Y. Lee, H. K. Kim, and S. W. Lee, "The Efficacy of Fibroblast Growth Factor for the Treatment of Chronic Vocal Fold Scarring: From Animal Model to Clinical Application," Clin. Exp. Otorhinolaryngol. **10**(4), 349–356 (2017).
37. A. Deniset-Besseau, J. Duboisset, E. Benichou, F. Hache, P.-F. Brevet, and M.-C. Schanne-Klein, "Measurement of the Second-Order Hyperpolarizability of the Collagen Triple Helix and Determination of Its Physical Origin," J. Phys. Chem. B **113**(40), 13437–13445 (2009).
38. P. Stoller, K. M. Reiser, P. M. Celliers, and A. M. Rubenchik, "Polarization-Modulated Second Harmonic Generation in Collagen," Biophys. J. **82**(6), 3330–3342 (2002).
39. F. Chen, P. W. Tillberg, and E. S. Boyden, "Expansion microscopy," Science **347**, 543–548 (2015).
40. P. P. Mondal and A. Diaspro, "Lateral resolution improvement in two-photon excitation microscopy by aperture engineering," Opt. Commun. **281**(7), 1855–1859 (2008).
41. B. C. Chen, W. R. Legant, K. Wang, L. Shao, D. E. Milkie, M. W. Davidson, C. Janetopoulos, X. S. Wu, J. A. Hammer 3rd, Z. Liu, B. P. English, Y. Mimori-Kiyosue, D. P. Romero, A. T. Ritter, J. Lippincott-Schwartz, L. Fritz-Laylin, R. D. Mullins, D. M. Mitchell, J. N. Bembenek, A. C. Reymann, R. Böhme, S. W. Grill, J. T. Wang, G. Seydoux, U. S. Tulu, D. P. Kiehart, and E. Betzig, "Lattice light-sheet microscopy: imaging molecules to embryos at high spatiotemporal resolution," Science **346**(6208), 1257998 (2014).
42. F. O. Fahrbach, V. Gurchenkov, K. Alessandri, P. Nassoy, and A. Rohrbach, "Light-sheet microscopy in thick media using scanned Bessel beams and two-photon fluorescence excitation," Opt. Express **21**(11), 13824–13839 (2013).
43. F. Cella Zanacchi, Z. Lavagnino, M. Faretta, L. Furia, and A. Diaspro, "Light-Sheet Confined Super-Resolution Using Two-Photon Photoactivation," PLoS One **8**(7), e67667 (2013).
44. A. Suehiro, J. M. Bock, J. E. Hall, C. G. Garrett, and B. Rousseau, "Feasibility and acute healing of vocal fold microflap incisions in a rabbit model," Laryngoscope **122**(3), 600–605 (2012).
45. L. Nolte, G. C. Antonopoulos, L. Rämisch, A. Heisterkamp, T. Ripken, and H. Meyer, "Enabling second harmonic generation as a contrast mechanism for optical projection tomography (OPT) and scanning laser optical tomography (SLOT)," Biomed. Opt. Express **9**(6), 2627–2639 (2018).